ELSEVIER

Comput. Methods Appl. Mech. Engrg. 190 (2000) 1407–1424

Computer methods in applied mechanics and engineering

www.elsevier.com/locate/cma

A compact monotonic discretization scheme for solving second-order vorticity–velocity equations

Tony W.H. Sheu [*], T.P. Chiang, S.M. Liou

Department of Naval Architecture and Ocean Engineering, National Taiwan University, 73 Chou-Shan Road, Taipei, Taiwan, ROC

Received 11 January 1999; received in revised form 30 June 1999

Abstract

This paper presents a numerical method for solving the steady-state Navier–Stokes equations for incompressible fluid flows using velocities and vorticity as working variables. The method involves solving a second-order differential equation for the velocity and a convection–diffusion equation for the vorticity in Cartesian grids. The key to the success of the numerical simulation of this class of flow equations depends largely on proper simulation of vorticity transport equation subject to proper boundary vorticity. In this paper, we present a monotonic advection–diffusion multi-dimensional scheme and a theoretically rigorous implementation of vorticity boundary conditions. While the derivation of the proposed integral vorticity boundary condition is more elaborate and is more difficult to solve than conventional local approaches, the present approach offers significant advantages. In this study, both lid-driven and backward-facing step problems have been selected for comparison and validation purposes. © 2000 Elsevier Science S.A. All rights reserved.

Keywords: Steady-state; Navier–Stokes equations; Incompressible; Vorticity boundary condition

1. Introduction

There have been many studies of practically important incompressible Navier–Stokes equations in the last three decades. The traditional approach to the numerical solution of this class of flows has been to solve working equations in velocity–pressure variables. A serious problem which was encountered while performing the primitive variable formulation is owing to the absence of pressure in the continuity equation. This destabilizes the differential system and poses computational difficulties in the mixed formulation. In addition, discretization of pressure gradients in the incompressible equations on curvilinear grids presents considerable difficulties owing to the fact that the approximation of pressure gradient operator should be irrotational [1]. While this difficulty can be effectively resolved on staggered grids [2], special care is needed when grids are non-uniformly and non-orthogonally laid on the flow [1]. It is the added grid complexity that complicates further the incompressible flow analysis.

Another popular approach to numerical solution of the Navier–Stokes equations is the velocity–vorticity approach. This formulation is the most appropriate choice for solving the vortex dominated flow. The reason lies in the fact that the advection of vorticity is the most important process determining the flow dynamics. Additionally, it appears that studying incompressible Navier–Stokes equations in terms of vorticity and velocity is closer to physical reality [3]. For further details concerning the main features of this formulation, the reader is referred to the book by Quartapelle [4] and the review paper by Gatski [5]. The

[*] Corresponding author. Tel.: +886-2-23625470; fax: +886-2-23929885.
E-mail address: sheu@indy.na.ntu.edu.tw (T.W.H. Sheu).

PII: S0045-7825(00)00169-9

advantages of adopting the velocity–vorticity formulation were also given by Speziale [6]. Since the pioneering work of Fasel [7], several integral [8] and differential [9–21] approaches have been devised. In the context of the differential approach, the velocity–vorticity formulation can be divided into two subgroups. The first group of approaches corresponds to solving the Cauchy–Riemann problem [11–14]. This problem consists of finding a divergence-free velocity vector $\underline{u}$ whose curl is known as the vorticity. When we treat the Cauchy–Riemann equations directly as a system of first-order partial differential equations, there is often a question as to whether there exists any constraint of grids to enable $\nabla \cdot \underline{u} = 0$ and $\nabla \times \underline{u} = \omega$ to be discretely satisfied. According to Huang and Li [22], it is very difficult, if not impossible, to obtain the discrete satisfaction of the divergence–curl (DC) relation on a fully non-staggered grid.

For the present spatial discretization on collocated grids, we abandon the DC problem and confine ourselves to the second-order Poisson equations to solve for vorticity components. Another second-order differential equation for the velocity scalar must be solved subject to proper boundary conditions, which are the subject of the present study. An accurate prediction of the transport of vorticity is another consideration. We will address this issue in the use of an exponential compact scheme for the flux discretization.

This paper is organized as follows. Section 2 presents the differential formulation of the problem. The differential system involves solving two Poisson equations for the velocity components and the advection–diffusion scalar transport equation for the vorticity. In Section 3, we employ a monotonicity-preserving compact finite-difference scheme to discretize the convection–diffusion transport equation in two-dimensions. In Section 4, we derive a theoretically rigorous vorticity boundary condition. We justify the use of this vorticity boundary condition in Section 5 through benchmark problems known as the lid-driven cavity and the backward-facing step problems. Finally, in Section 6, we summarize our main conclusions.

2. Mathematical formulation

The traditional approach to the numerical solution of incompressible Navier–Stokes equations has been the primitive-variable formulation. This involves solving the following momentum equations, subject to appropriate boundary conditions, and the divergence-free continuity equation:

$$\underline{u} \cdot \nabla \underline{u} = -\nabla p + \frac{1}{Re} \nabla^2 \underline{u}, \tag{1}$$

$$\nabla \cdot \underline{u} = 0. \tag{2}$$

In the above equation, $\underline{u}$ is the velocity vector, p is the pressure. The definition of the Reynolds number Re involves the density ρ and the kinematic viscosity v.

In the discretization of the pressure gradient term in Eq. (1), grid non-uniformity and non-orthogonality warrant specific consideration when conducting analyses on curvilinear staggered grids. The guideline for the discretization of the gradient operator for pressure should be irrotational and should add no vorticity to the flow [1]. To avoid this difficulty, one can directly eliminate the pressure gradient terms from the above equations by taking the curl of (1) and using the kinematic definition of the vorticity $\underline{\omega} = \nabla \times \underline{u}$. The resulting transport equation is derived as

$$\underline{u} \cdot \nabla \underline{\omega} - \underline{\omega} \cdot \nabla \underline{u} = \frac{1}{Re} \nabla^2 \underline{\omega}. \tag{3}$$

The vorticity stretching term, $\underline{\omega} \cdot \nabla \underline{u}$, represents the generation or destruction of vorticity due to the stretching or compression of the vortex line. As the space dimension decreases by one, the vortex stretching term vanishes in two-dimensional cases, and the resulting vorticity transport equation is reduced to a scalar equation for the vorticity component which is normal to the planar motion of the flow:

$$\underline{u} \cdot \nabla \omega = \frac{1}{Re} \nabla^2 \omega. \tag{4}$$

Since the above equation is considered as one of the working equations, the application scope is limited to two-dimensional problems.

Successful simulation of the above convection–diffusion equation in two-dimensions requires proper specification of the boundary vorticity to close the problem. This is a difficult task since no-slip condition for the velocity cannot be reformulated in equivalent conditions of boundary value type for the vorticity. Therefore, special methods, ranging from approximate techniques based on interpolation to more theoretically rigorous methods relying on the influence matrix method (or capacitance matrix technique) [9] and the application of vorticity integral conditions [4], have to be employed in order to determine the boundary vorticity. The present steady-state study was undertaken to provide a new method for numerical implementation of the boundary vorticity in two-dimensions.

Common to the vorticity-based formulation of incompressible Navier–Stokes equations is that they involve solving the transport equation for vorticity. We will now turn to determining the working equations for the velocity components. In the literature, there exist two major types of governing equations for the velocity components:

(1) *Cauchy–Riemann problem*: In this approach, the divergence-free constraint equation is solved together with the definition of the vorticity to obtain velocity components [12–14]:

$$\nabla \times \underline{u} = \omega, \tag{5}$$

$$\nabla \cdot \underline{u} = 0. \tag{6}$$

As Eqs. (5) and (6) show, one can also refer to the Cauchy–Riemann problem as the div–curl problem. According to Quartapelle [4], the above first-order velocity–vorticity formulation was proved to be equivalent to the set consisting of the equations given in (1) and (2), provided that the velocity vector $\underline{b}$ specified on the boundary satisfies the following compatibility condition:

$$\oint \underline{n} \cdot \underline{b} \, \mathrm{d}s = 0. \tag{7}$$

In the above, $\underline{n}$ is the unit vector normal to the boundary and ds denotes the length of an infinitesimal element of the boundary.

(2) *Poisson equation problem*: The working equations for the velocity components can also be obtained by taking the curl of the definition $\omega = \nabla \times \underline{u}$ and by using the continuity equation given in (2). The resulting second-order Poisson equations for velocity components u and v are derived, respectively, as

$$\nabla^2 u = -\omega_y, \tag{8}$$

$$\nabla^2 v = \omega_x. \tag{9}$$

The theoretical equivalence between this classical second-order velocity–vorticity formulation and the velocity–pressure formulation has been given. For the details, we refer to the paper by Daube et al. [23].

In this paper, we adopt the Poisson equation approach mainly because there exist well-established schemes for solving the classical problem comprising Eqs. (8) and (9). Another reason why we abandon the div–curl problem in favor of the second-order velocity–vorticity approach is the ambiguity as to whether the discrete Cauchy–Riemann relations can be retained on collocated grids [23]. From the programming point of view, we prefer to deal with the Poisson problem on collocated grids without invoking grid staggering complexities for the incompressible Navier–Stokes equations. A point worthy of note is that the transport equation for the vorticity (4) is a benchmark equation for the development of the multi-dimensional advection–diffusion flux discretization scheme.

3. Advection–diffusion scheme for the vorticity transport equation

Referring to the computational module shown in Fig. 1, the solution ϕ_p is approximated by

$$-\sum_{i=\mathrm{W,E,S,N,SE,NE,NW,SW}} A_i\phi_i + A_p\phi_p = 0. \tag{10}$$

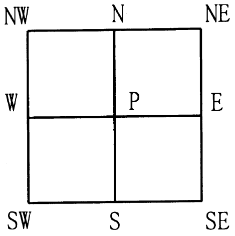

Fig. 1. Grid notation used in the development of the compact scheme.

Inspired by the idea of Patankar [24] who proposed the exponential scheme, we can incorporate the exponential nature of the general solution for Eq. (4) into the scheme development. By doing so, we assume that the above weighting coefficients A_i have the form:

$$A_{\mathrm{E}} = \alpha_1 \exp\left(-\frac{uh}{2}\right), \tag{11}$$

$$A_{\mathrm{W}} = \alpha_1 \exp\left(\frac{uh}{2}\right), \tag{12}$$

$$A_{\mathrm{N}} = \alpha_2 \exp\left(-\frac{vh}{2}\right), \tag{13}$$

$$A_{\mathrm{S}} = \alpha_2 \exp\left(\frac{vh}{2}\right), \tag{14}$$

$$A_{\mathrm{NE}} = \alpha_3 \exp\left(-\frac{uh+vh}{2}\right), \tag{15}$$

$$A_{\mathrm{SE}} = \alpha_3 \exp\left(\frac{-uh+vh}{2}\right), \tag{16}$$

$$A_{\mathrm{NW}} = \alpha_3 \exp\left(\frac{uh-vh}{2}\right), \tag{17}$$

$$A_{\mathrm{SW}} = \alpha_3 \exp\left(\frac{uh+vh}{2}\right), \tag{18}$$

$$A_P = -(A_{\mathrm{E}} + A_{\mathrm{W}} + A_{\mathrm{S}} + A_{\mathrm{N}} + A_{\mathrm{SW}} + A_{\mathrm{SE}} + A_{\mathrm{NE}} + A_{\mathrm{NW}}). \tag{19}$$

Our strategy for determining α_1, α_2 and α_3 is based on the modified equation analysis. The same idea has been used by Shay in his development of discretization scheme for Navier–Stokes equations [25]. After a considerable derivation in a domain covered with uniform grids with the size of $\Delta x = \Delta y = h$, the modified equation for Eq. (4) is derived as

$$u\omega_x + v\omega_y - \frac{1}{Re}(\omega_{xx} + \omega_{yy}) = a\omega_{xx} + b\omega_{yy} + c\omega_{xy} + H.O.T. \tag{20}$$

The left-hand side of Eq. (20) can be rederived provided that the following equations for α_1 and α_2 hold:

$$\alpha_1 = \frac{u}{2h\sinh\left(\frac{uh}{2}\right)} - 2\,\alpha_3\,\cosh\left(\frac{vh}{2}\right), \tag{21}$$

$$\alpha_2 = \frac{v}{2h\sinh\left(\frac{vh}{2}\right)} - 2\,\alpha_3\,\cosh\left(\frac{uh}{2}\right). \tag{22}$$

The normal diffusivities a and b and the skew diffusivity c shown in Eq. (20) are obtained as

$$a = \frac{uh}{2} \coth\left(\frac{uh}{2}\right), \tag{23}$$

$$b = \frac{vh}{2} \coth\left(\frac{vh}{2}\right), \tag{24}$$

$$c = 4h^2 \alpha_3 \ \sinh\left(\frac{vh}{2}\right) \ \sinh\left(\frac{uh}{2}\right). \tag{25}$$

As is apparent from Eqs. (21), (22) and (25), the key to success in this flux discretization development lies in determining the skew diffusivity c. Given that the monotonicity preserving property is crucial to avoid under- and over-shoots in regions of strong variation, a key issue that underlies this paper is to preserve the solution monotonicity. The idea behind acquiring solution monotonicity from an implicit scheme is the M-matrix theory [26,27] which demands that the coefficient matrix be irreducibly diagonal dominant. By definition, the matrix $[a_{ij}]_{n\times n}$ has the property of $|a_{ij}| > \sum_{i,j=1;i\neq j}^{n} |a_{ij}|$ for at least one i. As apparently revealed by Eq. (19), the compact scheme developed here is by no means a scheme which can provide monotonic solutions unless a small positive value ϵ (say $\epsilon = 10^{-7}$) is added to one of the matrix diagonals to make the coefficient matrix irreducibly diagonal dominant. Following the theorem given in [26,27], given an irreducibly diagonal dominant matrix $[a_{ij}]_{n\times n}$ with $a_{ij} \leqslant 0$ for all $i \neq j$ and $a_{ij} > 0$ for all $1 \leqslant i \leqslant n$, it follows that $\underline{\underline{A}}^{-1} > 0$. By definition, a non-singular real matrix whose entries a_{ij} are non-positive (i.e., $a_{ij} \leqslant 0$ for all $i \neq j$) and $\underline{\underline{A}}^{-1} > 0$, the matrix $\underline{\underline{A}}$ is called an M-matrix and the solutions $\underline{x}$ computed from $\underline{\underline{A}}\,\underline{x} = \underline{b}$ are unconditionally monotonic. We follow the underlying M-matrix theory to choose α_3 in order to satisfy the requirement of $a_{ij} < 0$ $(i \neq j)$:

$$\alpha_3 = \min\left(\frac{u}{2h\sinh(uh)}, \frac{v}{2h\sinh(vh)}\right). \tag{26}$$

In order to solve solutions from the 9-point stencil matrix equations, we adopt the modified strongly implicit procedure (MSIP) of Schneider and Zedan [28]. The use of the MSIP solver requires that an auxiliary matrix $\underline{\underline{P}}$ be added into the matrix equation $\underline{\underline{A}}$ to decompose the matrix $\underline{\underline{A}} + \underline{\underline{P}}$ into the product of $\underline{\underline{L}}$ and $\underline{\underline{U}}$ matrices as follows:

$$\underline{\underline{L}}\,\underline{\underline{U}}\,\underline{\phi}^{n+1} = \underline{\underline{P}}\,\underline{\phi}^{n}. \tag{27}$$

The resulting advantage can be clearly seen that finite-difference solutions ϕ can be obtained in two steps:

$$\textit{step } 1: \quad \underline{\underline{L}}\,\underline{V}^{n+1} = \underline{\underline{P}}\,\underline{\phi}^{n}, \tag{28}$$

$$\textit{step } 2: \quad \underline{\underline{U}}\,\underline{\phi}^{n+1} = \underline{V}^{n+1}. \tag{29}$$

The auxiliary matrix $\underline{\underline{P}}$ is chosen in such a way that the matrix $\underline{\underline{A}} + \underline{\underline{P}}$ has an $\underline{\underline{L}}\,\underline{\underline{U}}$ factorization, where the upper and lower triangular matrices retain the sparse structure as $\underline{\underline{A}}$ has. To accelerate the convergence of the solution, an adaptive optimization algorithm of Lage [29,30] is incorporated into MSIP.

We consider a scalar problem as a model to validate the compact monotonic scheme for the vorticity transport equation. The test problem is that of the skew advection–diffusion problem schematically shown in Fig. 2. In a square cavity of unit length, a titled line with an angle of $m = \tan^{-1}(v/u)$ passes through (0,0) and divides the cavity into two subdomains. Subject to the boundary condition given in Fig. 2, it is expected to have a marked change of ϕ across the dividing line. The velocity vector of magnitude 1 remains unchanged in the flow and is parallel to the dividing line. In this study, the square domain is uniformly discretized, resulting in a grid with $h = 0.05$. The fluid under investigation has a viscosity of $v = 10^{-4}$.

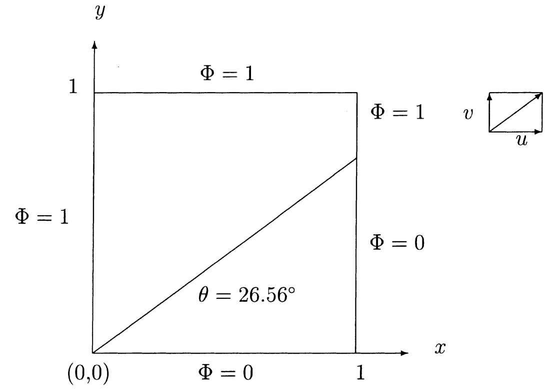

Fig. 2. A schematic of the skew advection–diffusion problem.

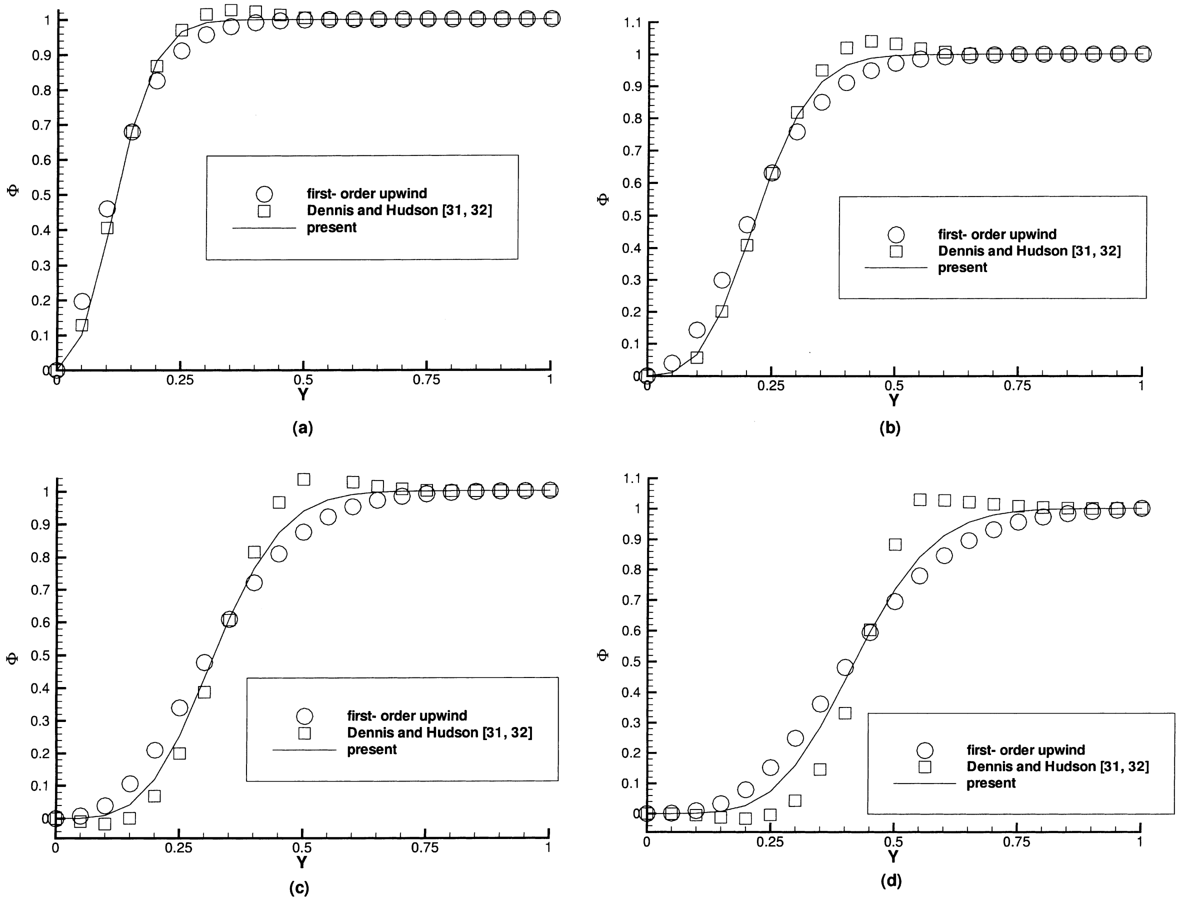

Fig. 3. The plot of ϕ at different x for showing the oscillation-free solution profiles: (a) $x = 0.2$; (b) $x = 0.4$; (c) $x = 0.6$; (d) $x = 0.8$.

As Fig. 3 reveals, oscillation-free solutions are observed in regions close to as well as away from the dividing line. Results computed from the first-order upwind scheme and the compact scheme of Dennis and Hudson [31,32] are also plotted for the comparison purposes. This example clearly demonstrates the suitability of using the proposed compact scheme to model problems involving steep gradients. To show that the M-matrix can be constructed using the present compact monotonic scheme, we plot weighting coefficients A_1–A_9 against Peclet numbers Pe_x and Pe_y in Fig. 4.

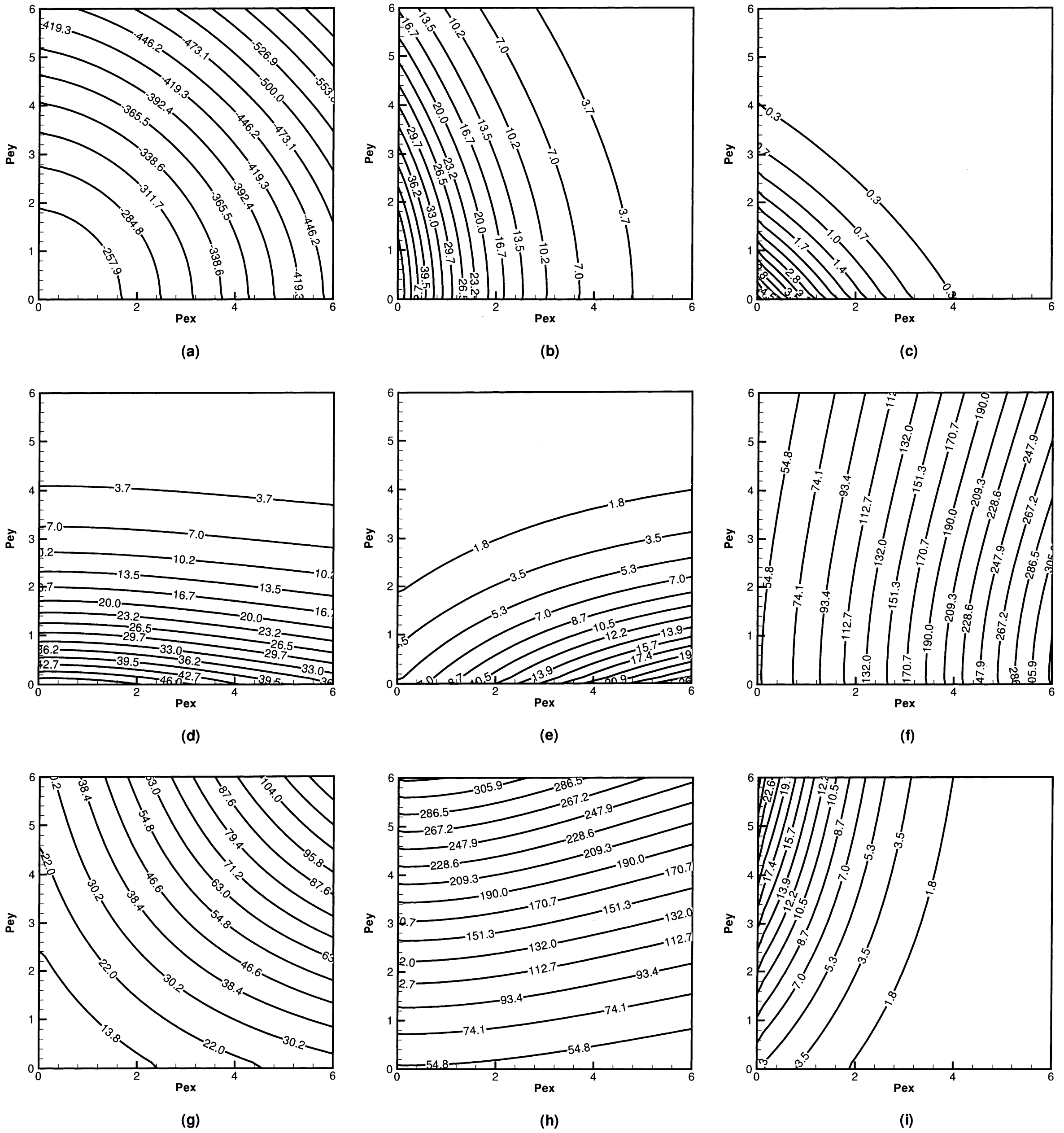

Fig. 4. Contour plots of A_1–A_9 against Peclet numbers Pe_x and Pe_y for the presently developed compact monotonic schemes: (a) A_1; (b) A_2; (c) A_3; (d) A_4; (e) A_5; (f) A_6; (g) A_7; (h) A_8; (i) A_9.

4. Vorticity integral condition

The key element in the vorticity–velocity formulation is to obtain the a priori unknown boundary values of the vorticity for the second-order transport Eq. (4). The theory behind our derivation of the vorticity boundary condition is the Green's identity, which relates two scalar potentials ϕ and ψ as follows:

$$\int_{\Omega} \phi\nabla^2\psi - \psi\nabla^2\phi \, \mathrm{d}A = \oint \left(\phi\frac{\partial\psi}{\partial n} - \psi\frac{\partial\phi}{\partial n} \right) \mathrm{d}s. \tag{30}$$

Provided that the scalar potential ψ is assigned as the stream function, the following two equations ensure satisfaction of mass conservation:

$$u = \frac{\partial \psi}{\partial y}, \tag{31}$$

$$v = -\frac{\partial \psi}{\partial x}. \tag{32}$$

It is addressed here that the present determination of vorticity boundary data limits the application scope to two-dimensions owing to the use of above definitions. Given the definition vorticity $\omega = \nabla \times \underline{u}$, we have

$$\nabla^2 \psi = -\omega. \tag{33}$$

Substitution of the above equation into (30) yields

$$-\int (\phi\omega + \psi\nabla^2\phi)\, \mathrm{d}A = \oint \left(\phi\frac{\partial \psi}{\partial n} - \psi\frac{\partial \phi}{\partial n} \right) \mathrm{d}s. \tag{34}$$

Now, let ϕ be the scalar potential which satisfies the Laplace equation. The boundary value of ϕ is enforced to be zero everywhere except at one point where the value is one.

$$\nabla^2 \phi = 0 \text{ in } \Omega, \tag{35}$$

$$\phi_i = \delta_{ij} \text{ on } \partial\Omega. \tag{36}$$

By virtue of Eqs. (35) and (36), Eq. (34) can be further simplified to

$$\int -\phi\omega\, \mathrm{d}A = \oint \left(\phi\frac{\partial \psi}{\partial n} - \psi\frac{\partial \phi}{\partial n} \right) \mathrm{d}s. \tag{37}$$

Let $\underline{Q}$ be $\psi\nabla\phi$, we can apply the divergence theorem on $\underline{Q}$ to yield

$$\int_\Omega \nabla \cdot \underline{Q}\, \mathrm{d}A = \int_{\partial\Omega} \underline{Q} \cdot \underline{n}\, \mathrm{d}s \tag{38}$$

or

$$\int_\Omega \nabla \cdot (\psi\nabla\phi)\, \mathrm{d}A = \int_{\partial\Omega} \psi\frac{\partial \phi}{\partial n}\, \mathrm{d}s. \tag{39}$$

By applying the identity $\nabla \cdot (\psi\nabla\phi) = \nabla\psi \cdot \nabla\phi + \psi\nabla^2\phi$, we have

$$\nabla \cdot (\psi\nabla\phi) = \nabla\psi \cdot \nabla\phi \tag{40}$$

through use of $\nabla^2\phi = 0$. The above equation enables us to simplify Eq. (39) to

$$\int_{\partial\Omega} \psi\frac{\partial \phi}{\partial n}\, \mathrm{d}s = \int_\Omega \nabla\phi \cdot \nabla\psi\, \mathrm{d}A. \tag{41}$$

As the above equation is used with the vector identity which involves the velocity u_τ that is tangential to the boundary

$$-\left.\frac{\partial \psi}{\partial n}\right|_{\partial\Omega} = u_\tau. \tag{42}$$

We can rewrite Eq. (37) as

$$\int_\Omega \phi\omega\, \mathrm{d}A = \oint_{\partial\Omega} \phi u_\tau\, \mathrm{d}s + \int_\Omega \left(v\frac{\partial \phi}{\partial x} - u\frac{\partial \phi}{\partial y} \right) \mathrm{d}A. \tag{43}$$

This completes the derivation of the vorticity integral equation for the transport Eq. (4).

It is worth noting that the assignment of $\phi = 1$ in Eq. (43) leads to

$$\int_{\Omega} \omega \, \mathrm{d}A = \oint_{\partial\omega} u_\tau \, \mathrm{d}s. \tag{44}$$

In the light of the above equation, the vorticity field in the computational domain should satisfy the integral condition expressing that the vorticity integrated over the domain is equal to the contour integral of the tangential component of the velocity along the boundary of the domain. In other words, the total vorticity solely depends on the circulation of the velocity along the periphery of the flow domain.

Without loss of generality we consider the mesh, shown schematically in Fig. 5, to describe the numerical implementation of the integral condition (43). To construct the matrix equation for the boundary solutions of $\omega_1, \omega_2 \ldots, \omega_{24}$, we divide the 20 boundary cells into two classes. The first class of cells is denoted by corner cells $\langle 1 \rangle, \langle 6 \rangle, \langle 11 \rangle$ and $\langle 16 \rangle$, as a shown in Fig. 6. In each corner cell, we apply the integral equation (44) to relate four vorticities. Taking the corner cell $\langle 1 \rangle$ as an example, we have

$$\omega_1 + \omega_2 + \omega_{24} = \frac{2}{h}(u_1 + u_2 - u_a - u_{24} + v_2 + v_a - v_1 - v_{24}) - \omega_a. \tag{45}$$

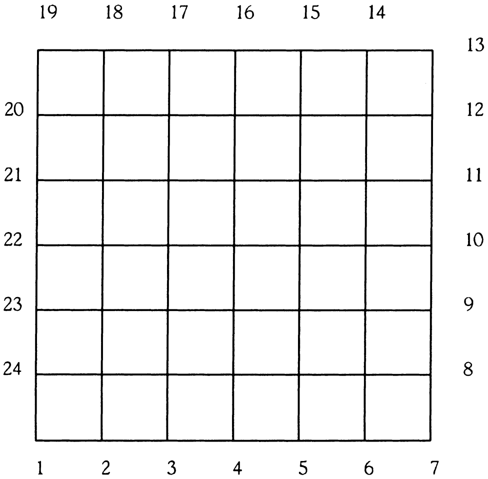

Fig. 5. Nodal assignment for the boundary vorticity in a domain covered by 36 elements.

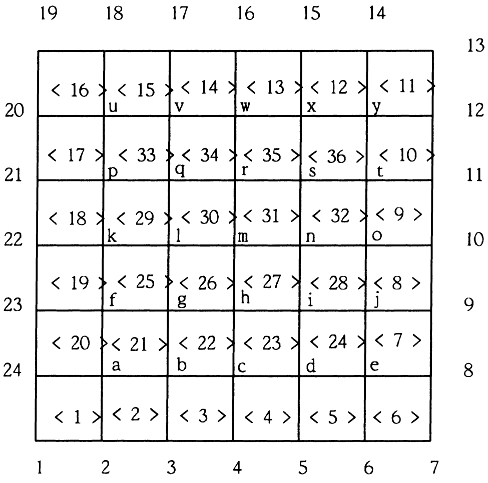

Fig. 6. Boundary cell assignment in a domain containing 36 elements.

For boundary cells other than corner cells, we apply the integral equation (43) in a region containing four cells. As an example, in a square containing elements $\langle 3\rangle, \langle 4\rangle, \langle 22\rangle$ and $\langle 23\rangle$, we can derive the following equation to relate the boundary vorticities $\omega_3, \omega_4,$ and ω_5 as follows:

$$\begin{aligned}
&C_1\omega_3 + (C_1 + C_2)\omega_4 + C_2\omega_5 \\
&\quad = -C_1\omega_b - (C_1 + C_2)\omega_c - C_2\omega_d - \left[\frac{\omega_b + \omega_g + \omega_h + \omega_c}{4}\right] \cdot \left[\frac{\phi_b + \phi_g + \phi_h + \phi_c}{4}\right] \\
&\qquad - \left[\frac{\omega_c + \omega_d + \omega_h + \omega_i}{4}\right] \cdot \left[\frac{\phi_c + \phi_d + \phi_h + \phi_i}{4}\right] \\
&\qquad + \left(\oint_{\partial\Omega} \phi u_\tau \, \mathrm{d}s + \int_\Omega \left(v\frac{\partial\phi}{\partial x} - u\frac{\partial\phi}{\partial y}\right) \mathrm{d}A\right) \Big/ (\Delta x \cdot \Delta y),
\end{aligned} \tag{46}$$

where $C_1 = (\phi_3 + \phi_4 + \phi_b + \phi_c)/4,\ C_2 = (\phi_4 + \phi_5 + \phi_c + \phi_d)/4$. Similar derivation is carried out cell-by-cell, starting with cell 234-abc-fgh, followed by cell 345-bcd-ghi,... 8 9 10-ejo-din ...., and ending at cell 22 23 24-kfa-lgb. We are in short of eight equations to close the algebraic system for the 24 boundary vorticities. For the purpose of closure, we apply Eq. (43) to eight 4-cell elements which are adjacent to the corner cells. Specific to the derivation of these eight equations is that the solution for ϕ is subject to the Kronecker data at the corner point "2" if the 4-cell elements $\langle 2\rangle, \langle 3\rangle, \langle 21\rangle, \langle 22\rangle$ are taken as an example. As a result of the above derivation, we can derive the matrix equation $(A)_{24\times 24}\,(\omega_1, \omega_2, \ldots, \omega_{24})^{\mathrm{T}} = (b_1, \ldots, b_{24})^{\mathrm{T}}$.

A check on the matrix equation $(A)_{24\times 24}$ shows that this matrix is nearly singular. Therefore, the boundary vorticities are very difficult to solve. To overcome this difficulty, we reformulate the matrix equation by taking ω_2 as the unknown while ω_3 and ω_4 are obtained by other means and are assigned to the right-hand side of the equation. The resulting source term b_2 takes the following form:

$$\begin{aligned}
b_2 = &- (C_1 + C_2)\omega_3 - C_2\omega_4 - C_1\omega_a - (C_1 + C_2)\omega_b - C_2\omega_c - \left[\frac{\omega_a + \omega_f + \omega_g + \omega_b}{4}\right] \\
&\cdot \left[\frac{\phi_a + \phi_f + \phi_g + \phi_b}{4}\right] - \left[\frac{\omega_b + \omega_c + \omega_g + \omega_h}{4}\right] \cdot \left[\frac{\phi_b + \phi_c + \phi_g + \phi_h}{4}\right] \\
&+ \left(\oint_{\partial\Omega} \phi u_\tau \, \mathrm{d}s + \int_\Omega \left(v\frac{\partial\phi}{\partial x} - u\frac{\partial\phi}{\partial y}\right) \mathrm{d}A\right) \Big/ (\Delta x \cdot \Delta y),
\end{aligned} \tag{47}$$

where $C_1 = (\phi_2 + \phi_3 + \phi_a + \phi_b)/4$, $C_2 = (\phi_3 + \phi_4 + \phi_b + \phi_c)/4$, $\omega_3 = ((v_4 - v_2)/(2\Delta x)) - (-u_g + 4u_b - 3u_3)/(2\Delta y)$ and $\omega_4 = ((v_5 - v_3)/(2\Delta x)) - ((-u_h + 4u_c - 3u_4)/(2\Delta y))$. Following the same idea as that given above, other source terms b_6, b_8, b_{12}, b_{14}, b_{18}, b_{20}, and b_{24} can be derived and are summarized in the Appendix A for the sake of completeness.

5. Numerical studies

5.1. Lid-driven cavity flow problem

Research into the lid-driven cavity flow structure is an area of continuing interest and was selected as a benchmark problem for a major international workshop [33]. This problem has attracted considerable attention because this flow configuration is relevant to many industrial applications. The geometrical simplicity facilitates experimental calibrations or numerical implementation and, thus, provides benchmark data for comparison and validation. The flow physics inside this cavity are, however, by no means simple. Several flow characteristics which prevail in processing industries, such as boundary layers, eddies of different sizes and characters, and various instabilities, may coexist.

In this section, we present a two-dimensional simulation for the fluid flow in a square cavity defined by $B : D = 1 : 1$. The Reynolds numbers chosen for this study were 400 and 1000, which were computed based on the lid speed, the width of the cavity, and the kinematic viscosity of the fluid. As shown in Fig. 7, this cavity is subject to a lid motion at the upper plane. In this study, the solutions were computed on uniform

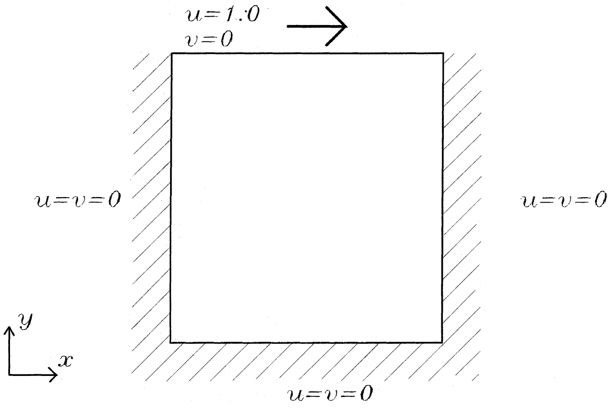

Fig. 7. A schematic of the lid-driven cavity problem considered in Section 5.1.

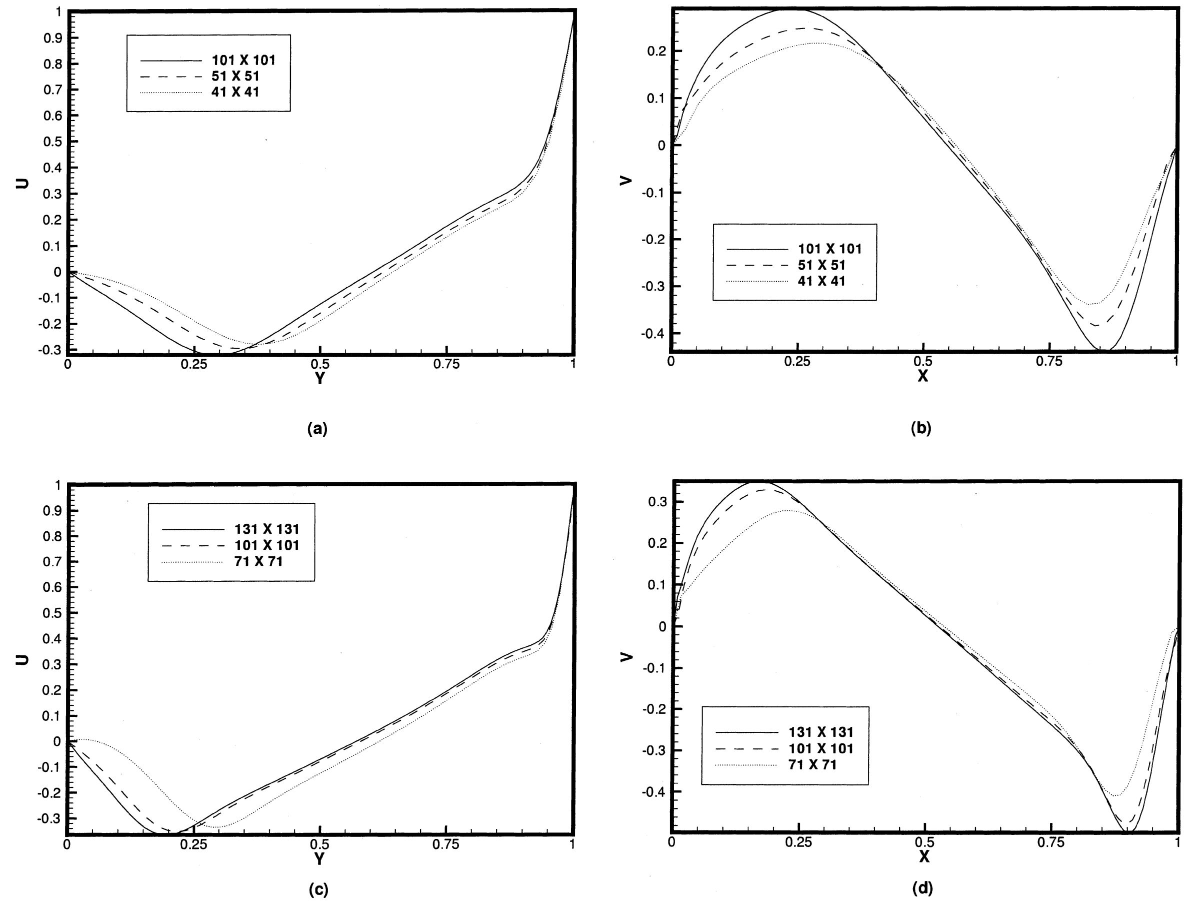

(a)

(b)

(c)

(d)

Fig. 8. Grid convergence tests for the lid-driven cavity flow problems computed at $Re = 400$ and 1000. (a) $u(x = 0.5,\ y,\ Re = 400)$; (b) $v(x,\ y = 0.5,\ Re = 400)$; (c) $u(x = 0.5,\ y,\ Re = 1000)$; (d) $v(x, y = 0.5,\ Re = 1000)$;.

grids of different resolutions. Through grid convergence tests, it is clearly seen from Fig. 8 that solutions computed under 101 × 101 for $Re = 400$ while 131 × 131 for $Re = 1000$ provide grid independent solutions. We determined the vortex centers of different kinds shown in Fig. 9 and tabulated them together with data computed by Ghia et al. [34] in Table 1. A comparison was made by plotting the velocity profiles along the centerlines in Fig. 10 for the case $Re = 400$ and in Fig. 11 for a higher Reynolds number, $Re = 1000$. For comparison purpose, the velocity profiles of Ghia et al. [34] are also plotted in Figs. 10 and 11.

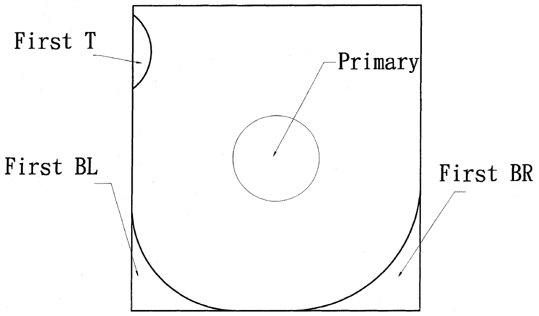

Fig. 9. An illustration of different types of vortex in the lid-driven cavity.

Table 1
Comparison of cavity problem for Ghia et al. [34] and present[a]

ω location (x,y)	$Re = 400$	$Re = 1000$
Primary	0.5579, 0.6119 (0.5547, 0.6055)	0.5331, 0.5745 (0.5313, 0.5625)
First BL	0.0548, 0.0438 (0.0508, 0.0469)	0.0821, 0.0754 (0.0859, 0.0781)
First BR	0.88, 0.126 (0.8906, 0.125)	0.8542, 0.1187 (0.8594, 0.1094)
Grid size	101 × 101 (257 × 257)	130 × 130 (129 × 129)

[a] Remark: ( ) is Ghia et al. [34] computational value.

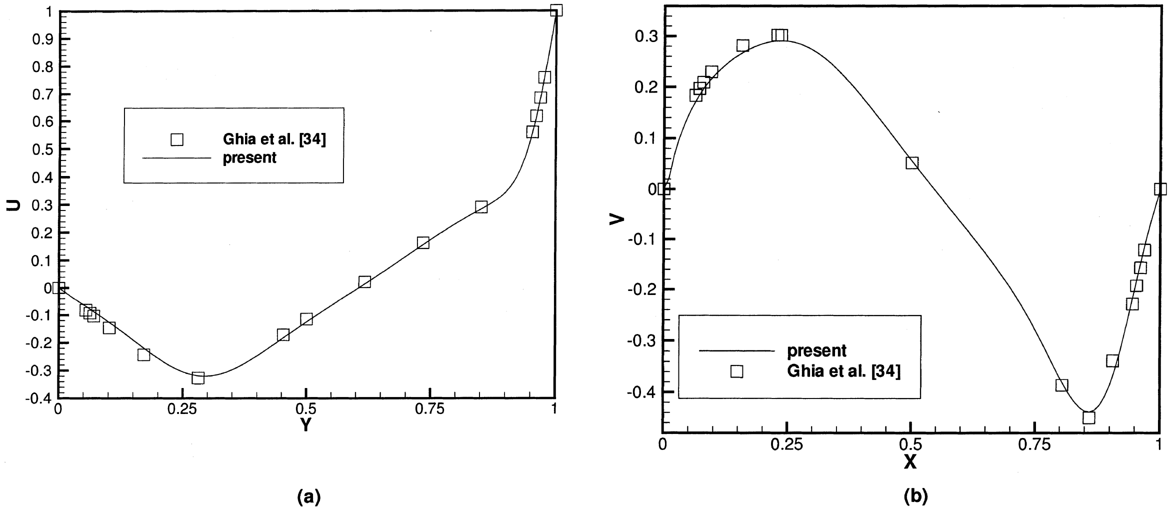

Fig. 10. Velocity profiles plotted on the centerlines for the case $Re = 400$ (a) u–y plot at $x = 0.5$; (b) v–x plot at $y = 0.5$.

5.2. Backward-facing step problem

Expansion flows in straight channels with steps have been another focus of intensive study over the last few decades and have been the subject of an international workshop [35]. Although this flow represents one of the simplest expansion flows, the physics involved are rather complex due to the formation of

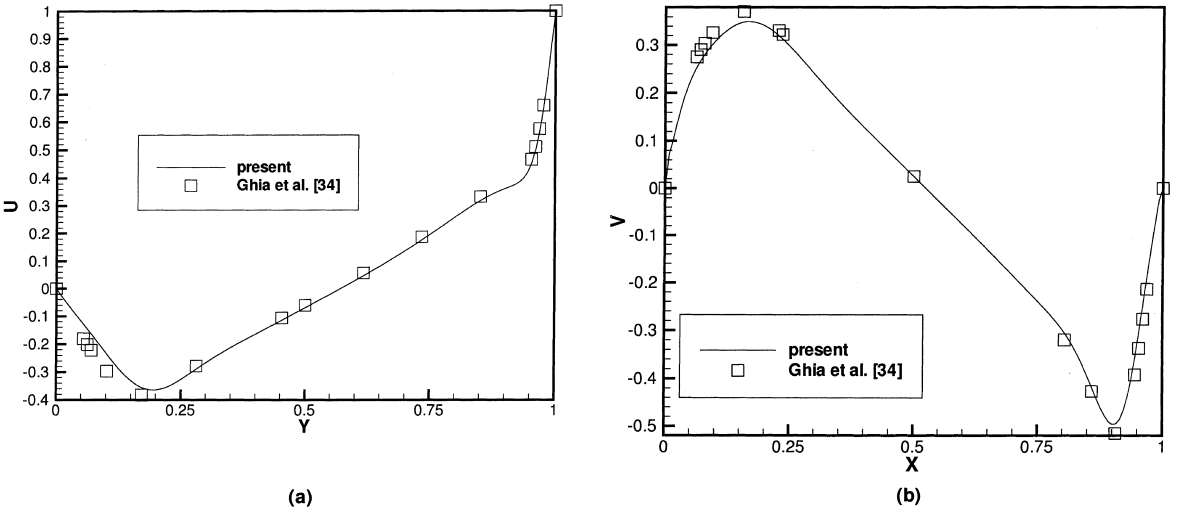

Fig. 11. Velocity profiles plotted on the centerlines for the case $Re = 1000$ (a) u–y plot at $x = 0.5$; (b) v–x plot at $y = 0.5$.

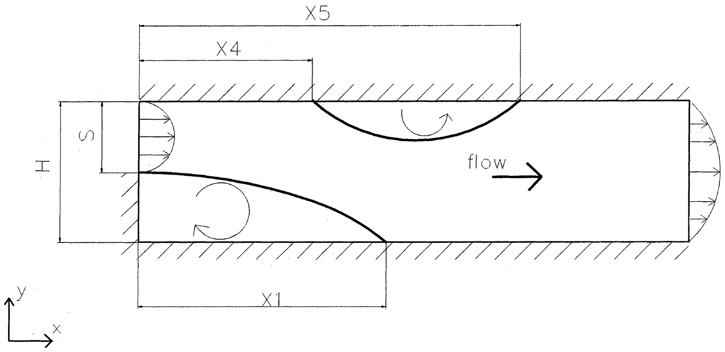

Fig. 12. Schematic of the backward-facing step problem considered in Section 5.2.

recirculating vortices and flow reversals downstream of the step. We consider this problem to be computationally important because of the availability of experimental data [33,34] and the simplicity of the geometry.

Several Reynolds numbers, $Re = 100$, 200, 400, 500 and 800, were considered in this study. Among the basic features pertinent to the problem, as illustrated in Fig. 12, is the flow separation from the step corner. As in many real flows, separation of a boundary layer is followed by downstream reattachment to a solid wall. Determining the reattachment location, as measured from the step, is, thus, the primary focus of this study. It is also important to see the separation–reattachment eddy on the channel roof.

Notwithstanding, the importance of eddy formation in the channel, we plot reattachment lengths of the primary eddy behind the step in Fig. 13 for cases with different Reynolds numbers. We compared our results with measurement data [36] as well as other numerical data [37,38] for the sake of completeness. We also plot the separation length of the roof eddy in Fig. 14 and compare results with experimental [36] and numerical [37] data for the Reynolds numbers considered in this study. Fig. 15 plots the reattachment location of the roof eddy together with data given by Armaly et al. [36] and Gartling [37]. From this comparison, it is now considered that our compact scheme is applicable to Navier–Stokes flow simulations of the vortical flow structure.

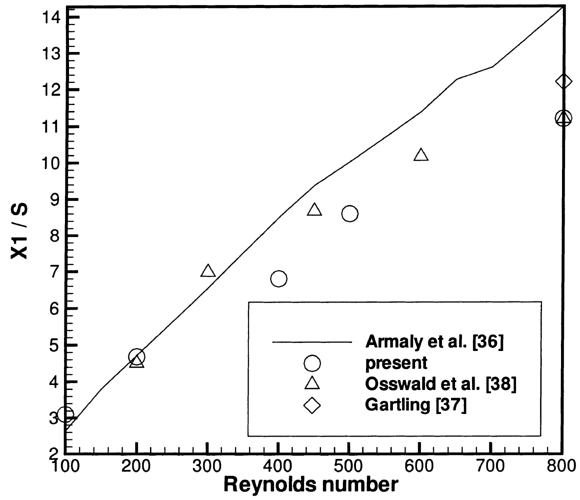

Fig. 13. The reattachment locations, x_1, on the floor of the channel versus *Re*.

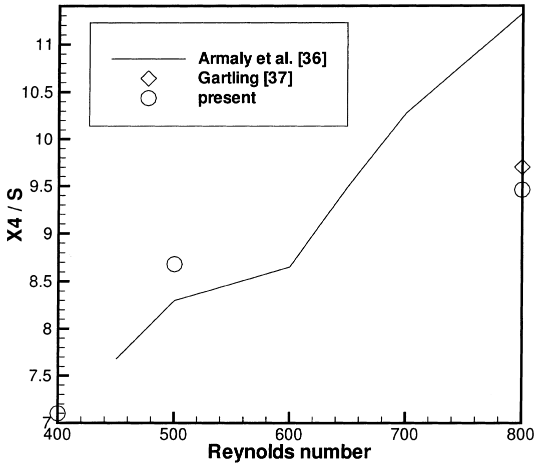

Fig. 14. The separation locations, x_4, on the roof of the channel against *Re*.

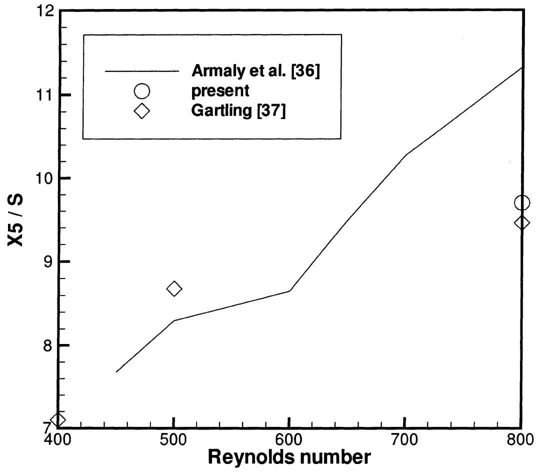

Fig. 15. The reattachment locations, x_5, on the floor of the channel against *Re*.

6. Concluding remarks

The goal for the present study was to simulate incompressible viscous flows by means of the velocity–vorticity formulation. In order for the solutions to be accurately predicted, it is important to develop a theoretically rigorous framework which can provide us with boundary vorticity without using field variables outside of the physical domain. The equation governing the boundary vorticity is derived in integral form. Thus, boundary vorticities are simultaneously solved from the matrix equation. The two-dimensional solution algorithm involves a scalar transport equation for the vorticity variable and two Poisson equations for velocity components. We pay special attention to numerical simulation of the convection–diffusion equation for the transport of vorticity. It is demanded that the solutions computed be monotonic. In the development of compact scheme, we take the exponential nature of the solution of the convection–diffusion equation into consideration. Specific to our flux discretization scheme is that the coefficient matrix of the compact 9-point stencil scheme is classified as an irreducibly diagonal dominant M-matrix. To better understand the compact finite-difference scheme developed here, we have conducted the lid-driven cavity and the backward-facing step problems. The results demonstrate that the integral approach designed to provide the boundary vorticity is applicable to simulation of fluid flows which are vortical in nature.

Acknowledgements

This author would like to thank the Computer Center of National Taiwan University and the National Center for High-performance Computing (NCHC) for providing CRAY J916 and IBMRS/6000-590 computers, which made this study possible. Research support provided by the National Science Council under Grant NSC87-2213-E-002-002 is also gratefully acknowledged.

Appendix A

$$\begin{aligned} b_6 = &- C_1\omega_4 - (C_1 + C_2)\omega_5 - C_1\omega_c - (C_1 + C_2)\omega_d - C_2\omega_e - \left[\frac{\omega_c + \omega_h + \omega_i + \omega_d}{4}\right] \\ &\cdot \left[\frac{\phi_c + \phi_h + \phi_i + \phi_d}{4}\right] - \left[\frac{\omega_d + \omega_i + \omega_j + \omega_e}{4}\right] \cdot \left[\frac{\phi_d + \phi_i + \phi_j + \phi_e}{4}\right] \\ &+ \left(\oint_{\partial\Omega} \phi u_\tau \, \mathrm{d}s + \int_\Omega \left(v\frac{\partial\phi}{\partial x} - u\frac{\partial\phi}{\partial y}\right) \mathrm{d}A\right) \Big/ (\Delta x \cdot \Delta y), \end{aligned} \tag{A.1}$$

where $C_1 = (\phi_4 + \phi_5 + \phi_c + \phi_d)/4$, $C_2 = (\phi_5 + \phi_6 + \phi_d + \phi_e)/4$, $\omega_4 = ((v_5 - v_3)/(2\Delta x)) - ((-u_h + 4u_c - 3u_4)/(2\Delta y))$, $\omega_5 = ((v_6 - v_4)/(2\Delta x)) - ((-u_i + 4u_d - 3u_5)/(2\Delta y))$.

$$\begin{aligned} b_8 = &- (C_1 + C_2)\omega_9 - C_2\omega_{10} - C_1\omega_e - (C_1 + C_2)\omega_j - C_2\omega_o - \left[\frac{\omega_d + \omega_e + \omega_i + \omega_j}{4}\right] \\ &\cdot \left[\frac{\phi_d + \phi_e + \phi_i + \phi_j}{4}\right] - \left[\frac{\omega_i + \omega_j + \omega_n + \omega_o}{4}\right] \cdot \left[\frac{\phi_i + \phi_j + \phi_n + \phi_o}{4}\right] \\ &+ \left(\oint_{\partial\Omega} \phi u_\tau \, \mathrm{d}s + \int_\Omega \left(v\frac{\partial\phi}{\partial x} - u\frac{\partial\phi}{\partial y}\right) \mathrm{d}A\right) \Big/ (\Delta x \cdot \Delta y), \end{aligned} \tag{A.2}$$

where $C_1 = (\phi_e + \phi_j + \phi_8 + \phi_9)/4$, $C_2 = (\phi_j + \phi_o + \phi_9 + \phi_{10})/4$, $\omega_9 = ((v_i - 4v_j + 3v_9)/(2\Delta x))((-u_{10} - u_8)/(2\Delta y))$, $\omega_{10} = ((v_n - 4v_o + 3v_{10})/(2\Delta x)) - ((u_{11} - u_9)/(2\Delta y))$.

$$\begin{aligned} b_{12} = &- (C_1 + C_2)\omega_{11} - C_1\omega_{10} - C_1\omega_o - (C_1 + C_2)\omega_t - C_2\omega_y - \left[\frac{\omega_n + \omega_s + \omega_t + \omega_o}{4}\right] \\ &\cdot \left[\frac{\phi_n + \phi_s + \phi_t + \phi_o}{4}\right] - \left[\frac{\omega_s + \omega_t + \omega_x + \omega_y}{4}\right] \cdot \left[\frac{\phi_s + \phi_t + \phi_x + \phi_y}{4}\right] \\ &+ \left(\oint_{\partial\Omega} \phi u_\tau \, \mathrm{d}s + \int_\Omega \left(v\frac{\partial\phi}{\partial x} - u\frac{\partial\phi}{\partial y}\right) \mathrm{d}A\right) \Big/ (\Delta x \cdot \Delta y), \end{aligned} \tag{A.3}$$

where $C_1 = (\phi_o + \phi_t + \phi_{10} + \phi_{11})/4$, $C_2 = (\phi_t + \phi_y + \phi_{11} + \phi_{12})/4$, $\omega_{11} = ((v_s - 4v_t + 3v_{11})/(2\Delta x)) - ((u_{12} - u_{10})/(2\Delta y))$, $\omega_{10} = ((v_n - 4v_o + 3v_{10})/(2\Delta x)) - ((u_{11} - u_9)/(2\Delta y))$.

$$\begin{aligned} b_{14} = &- (C_1 + C_2)\omega_{15} - C_2\omega_{16} - C_1\omega_y - (C_1 + C_2)\omega_x - C_2\omega_w - \left[\frac{\omega_r + \omega_w + \omega_s + \omega_x}{4}\right] \\ &\cdot \left[\frac{\phi_r + \phi_w + \phi_s + \phi_x}{4}\right] - \left[\frac{\omega_s + \omega_t + \omega_x + \omega_y}{4}\right] \cdot \left[\frac{\phi_s + \phi_t + \phi_x + \phi_y}{4}\right] \\ &+ \left(\oint_{\partial\Omega} \phi u_\tau \, \mathrm{d}s + \int_\Omega \left(v\frac{\partial\phi}{\partial x} - u\frac{\partial\phi}{\partial y} \right) \mathrm{d}A \right) \Big/ (\Delta x \cdot \Delta y), \end{aligned} \tag{A.4}$$

where $C_1 = (\phi_{14} + \phi_{15} + \phi_x + \phi_y)/4$, $C_2 = (\phi_{15} + \phi_{16} + \phi_x + \phi_w)/4$, $\omega_{15} = ((v_{14} - v_{16})/(2\Delta x)) - ((u_s - 4u_x + 3u_{15})/(2\Delta y))$, $\omega_{16} = ((v_{15} - v_{17})/(2\Delta x)) - ((u_r - 4u_w + 3u_{16})/(2\Delta y))$.

$$\begin{aligned} b_{18} = &- (C_1 + C_2)\omega_{17} - C_1\omega_{16} - C_1\omega_w - (C_1 + C_2)\omega_v - C_2\omega_u - \left[\frac{\omega_u + \omega_v + \omega_p + \omega_q}{4}\right] \\ &\cdot \left[\frac{\phi_u + \phi_v + \phi_p + \phi_q}{4}\right] - \left[\frac{\omega_v + \omega_w + \omega_q + \omega_r}{4}\right] \cdot \left[\frac{\phi_v + \phi_w + \phi_q + \phi_r}{4}\right] \\ &+ \left(\oint_{\partial\Omega} \phi u_\tau \, \mathrm{d}s + \int_\Omega \left(v\frac{\partial\phi}{\partial x} - u\frac{\partial\phi}{\partial y} \right) \mathrm{d}A \right) \Big/ (\Delta x \cdot \Delta y), \end{aligned} \tag{A.5}$$

where $C_1 = (\phi_{16} + \phi_{17} + \phi_v + \phi_w)/4$, $C_2 = (\phi_{17} + \phi_{18} + \phi_u + \phi_v)/4$, $\omega_{17} = ((v_{16} - v_{18})/(2\Delta x)) - ((+u_q - 4u_v + 3u_{17})/(2\Delta y))$, $\omega_{16} = ((v_{15} - v_{17})/(2\Delta x)) - ((+u_r - 4u_w + 3u_{16})/(2\Delta y))$.

$$\begin{aligned} b_{20} = &- (C_1 + C_2)\omega_{21} - C_2\omega_{22} - C_1\omega_u - (C_1 + C_2)\omega_p - C_2\omega_k - \left[\frac{\omega_u + \omega_v + \omega_p + \omega_q}{4}\right] \\ &\cdot \left[\frac{\phi_u + \phi_v + \phi_p + \phi_q}{4}\right] - \left[\frac{\omega_p + \omega_q + \omega_k + \omega_l}{4}\right] \cdot \left[\frac{\phi_p + \phi_q + \phi_k + \phi_l}{4}\right] \\ &+ \left(\oint_{\partial\Omega} \phi u_\tau \, \mathrm{d}s + \int_\Omega \left(v\frac{\partial\phi}{\partial x} - u\frac{\partial\phi}{\partial y} \right) \mathrm{d}A \right) \Big/ (\Delta x \cdot \Delta y), \end{aligned} \tag{A.6}$$

where $C_1 = (\phi_{20} + \phi_{21} + \phi_p + \phi_u)/4$, $C_2 = (\phi_{21} + \phi_{22} + \phi_p + \phi_k)/4$, $\omega_{21} = ((-v_q + 4v_p - 3v_{21})/(2\Delta x)) - ((u_{20} - u_{22})/(2\Delta y))$, $\omega_{22} = ((-v_1 + 4v_k - 3v_{22})/(2\Delta x)) - ((u_{21} - u_{23})/(2\Delta y))$.

$$\begin{aligned} b_{24} = &- (C_1 + C_2)\omega_{23} - C_1\omega_{22} - C_1\omega_k - (C_1 + C_2)\omega_f - C_2\omega_a - \left[\frac{\omega_a + \omega_b + \omega_f + \omega_g}{4}\right] \\ &\cdot \left[\frac{\phi_a + \phi_b + \phi_f + \phi_g}{4}\right] - \left[\frac{\omega_f + \omega_g + \omega_k + \omega_l}{4}\right] \cdot \left[\frac{\phi_f + \phi_g + \phi_k + \phi_l}{4}\right] \\ &+ \left(\oint_{\partial\Omega} \phi u_\tau \, \mathrm{d}s + \int_\Omega \left(v\frac{\partial\phi}{\partial x} - u\frac{\partial\phi}{\partial y} \right) \mathrm{d}A \right) \Big/ (\Delta x \cdot \Delta y), \end{aligned} \tag{A.7}$$

where $C_1 = (\phi_{22} + \phi_{23} + \phi_k + \phi_f)/4$, $C_2 = (\phi_{23} + \phi_{24} + \phi_f + \phi_a)/4$, $\omega_{23} = ((-v_g + 4v_f - 3v_{23})/(2\Delta x)) - ((u_{22} - u_{24})/(2\Delta y))$, $\omega_{22} = ((-v_1 + 4v_k - 3v_{22})/(2\Delta x)) - ((u_{21} - u_{23})/(2\Delta y))$.

References

[1] R.S. Bernard, H. Kapitza, How to discretize the pressure gradient for curvilinear MAC grids, J. Comput. Phys. 99 (1992) 288–298.

[2] E. Wienan, J.-G. Liu, Finite-difference methods for 3D viscous incompressible flows in the vorticity–vector potential formulation on non-staggered grids, J. Comput. Phys. 138 (1997) 57–82.

[3] H.J.H. Clercx, A spectral solver for the Navier–Stokes equations in the velocity–vorticity formulation for flows with two non-periodic directions, J. Comput. Phys. 137 (1997) 186–211.

[4] L. Quartapelle, Numerical solution of the incompressible Navier–Stokes equations, Birkhauser, Basel, 1993.

[5] T.B. Gatski, Review of incompressible fluid flow computations using the vorticity–velocity formulation, Appl. Numer. Math. 7 (1991) 227–239.

[6] C.G. Speziale, On the advantages of the vorticity–velocity formulation of the equations of fluid dynamics, J. Comput. Phys. 73 (1987) 476–480.

[7] H. Fasel, Investigation of the stability of boundary layers by a finite-difference model of the Navier–Stokes equations, J. Fluid Mech. 78 (2) (1976) 355–383.

[8] J.C. Wu, J.F. Thompson, Numerical solution of time-dependent incompressible Navier–Stokes equations using an integral–differential formulation, Comput. Fluids 1 (1973) 197–215.

[9] O. Daube, Resolution of the 2D Navier–Stokes equations in velocity– vorticity form by means of an influence matrix technique, J. Comput. Phys. 103 (1992) 402–414.

[10] P. Giannattasio, M. Napolitano, Optimal vorticity conditions for the node-centred finite-difference discretization of the second-order vorticity–velocity equations, J. Comput. Phys. 127 (1996) 208–217.

[11] F. Bertagnolio, O. Daube, Solution of the div–curl problem in generalized curvilinear coordinates, J. Comput. Phys. 138 (1997) 121–152.

[12] T.B. Gatski, C.E. Grosch, M.E. Rose, The numerical solution of the Navier–Stokes equations for 3-dimensional unsteady incompressible flows by compact schemes, J. Comput. Phys. 82 (1989) 298–329.

[13] Y. Huang, V. Ghia, G.A. Osswald, K.N. Ghia, Velocity–vorticity simulation of unsteady 3D viscous flow within a driven cavity, in: M. Deville, T.H. Le, Y. Morchoisne (Ed.), Notes on Numerical Fluid Mechanics, vol. 36, Vieweg, Braunschweig, 1992.

[14] G.A. Osswald, K.N. Ghia, U. Ghia, A direct algorithm for solution of incompressible three-dimensional Navier–Stokes equations, in: AIAA Eighth Computational Fluid Dynamics Conference, Honolulu, HI, 1987, pp. 408–421.

[15] S.C.R. Dennis, D.B. Ingham, R.N. Cook, Finite-difference methods for calculating steady incompressible flows in three dimensions, J. Comput. Phys. 33 (1979) 325–339.

[16] T.B. Gatski, L.E. Grosch, M.E. Rose, A numerical study of the two-dimensional Navier–Stokes equations in vorticity–velocity varriables, J. Comput. Phys. 48 (1982) 1–22.

[17] T.B. Gatski, L.E. Grosch, M.E. Rose, The numerical solution of the Navier–Stokes equations for 3-dimensional unsteady incompressible flows by compact schemes, J. Comput. Phys. 82 (1989) 298–329.

[18] M. Napolitano, L.A. Catalano, A multi-grid solver for the vorticity–velocity Navier–Stokes equations, Int. Numer. Meth. Fluids 13 (1991) 49–59.

[19] M. Napolitano, G. Pascazio, A numerical method for the vorticity–velocity Navier–Stokes equations in two and three dimensions, Comput. Fluids 19 (3/4) (1991) 489–495.

[20] P. Orlandi, Vorticity–velocity formulation for high *Re* flow, Comput. Fluids 15 (2) (1987) 137–149.

[21] G. Gui, F. Stella, A vorticity–velocity method for the numerical solution of 3D incompressible flows, J. Comput. Phys. 106 (1993) 286–298.

[22] H. Huang, M. Li, Finite-difference approximation for the velocity–vorticity formulation on staggered and non-staggered grids, Comput. Fluids 26 (1) (1997) 59–82.

[23] O. Daube, J.C. Guermond, A. Sellier, Sur la formulation vitesse-toubillon des equations de Navier–Stokes en ecoulement incompressible, C.R. Acad. Sci. Paris 313 (serie II) (1991) 377–382.

[24] S.V. Patankar, Numerical Heat Transfer and Fluid Flow, Hemisphere, Washington DC, 1980.

[25] W.A. Shay, Development of a second-order approximation for the Navier–Stokes equations, Comput. Fluids 9 (1981) 279–298.

[26] T. Meis, U. Marcowitz, Numerical solution of partial differential equations, in: Applied Mathematical Science, vol. 32, Springer, Berlin, 1981.

[27] T. Ikeda, Maximal principle in finite-element models for convection–diffusion phenomena, in: Numerical and Applied Analysis, vol. 4, North-Holland, Kinokuniya, Amsterdam, Tokyo, 1983.

[28] G.E. Schneider, M. Zedan, A modified strongly implicit procedure for numerical solution of field problem, Numer. Heat Transfer 4 (1981) 1–19.

[29] P.L.C. Lage, Application of the optimized modified strongly implicit procedure to nonlinear problems, Numer. Heat Transfer B 30 (1996) 423–435.

[30] P.L.C. Lage, Adaptive optimization of the iteration parameter in the modified strongly implicit procedure, Numer. Heat Transfer B 30 (1996) 255–270.

[31] S.C.R. Dennis, J.D. Hudson, Compact h^4 finite-difference approximation to operators of Navier–Stokes type, J. Comput. Phys. 85 (1989) 390–416.

[32] S.C.R. Dennis, J.D. Hudson, An h^4 accurate vorticity–velocity formulation for calculating flow past a cylinder, Int. J. Numer. Methods Fluids 21 (1995) 489–497.

[33] M. Deville, T.H.Lê, Y. Morchoisneceds, Numerical Simulation of 3D Incompressible Unsteady Viscous Laminar Flowss, vol. 36, NNFM, 1992.

[34] U. Ghia, K.N. Ghia, C.T. Shin, High-Re solutions for incompressible flow using the Navier–Stokes equations and a multigrid method, J. Comput. Phys. 48 (1982) 387–411.

[35] K. Morgan, J. Periaux, F. Thomasset (Eds.), Analysis of Laminar Flow over a Backward-Facing Step, A GAMM-Workshop, Friedr Viewly and Sohn, Germany, 1984.

[36] B.F. Armaly, F. Durst, J.C.F. Pereira, B. Schönung, Experimental and theoretical investigation of backward-facing step flow, J. Fluid Mech. 127 (1983) 473–496.

[37] D.K. Gartling, A test problem for outflow boundary conditions – Flow over a backward-facing step, Int. J. Numer. Fluid 11 (1990) 953–967.

[38] G.A. Osswald, K.N. Ghia, U. Ghia, Study of incompressible separated flow using an implicit time-dependent technique, in: AIAA, Sixth CFD Conference, vol. 686, Denver, MA, 1983.